Finite Element Modeling and Simulation of a Robotic Finger Actuated by Ni-Ti Shape Memory Alloy Wires

Conference Paper · March 2019

DOI: 10.1117/12.2513919

CITATION
1

READS
305

5 authors, including:

Filomena Simone
Universität des Saarlandes
20 PUBLICATIONS **180** CITATIONS
SEE PROFILE

Daniele Meli
University of Verona
21 PUBLICATIONS **153** CITATIONS
SEE PROFILE

Gianluca Rizzello
Universität des Saarlandes
182 PUBLICATIONS **1,671** CITATIONS
SEE PROFILE

David Naso
Politecnico di Bari
208 PUBLICATIONS **4,018** CITATIONS
SEE PROFILE

Finite Element Modeling and Simulation of a Robotic Finger Actuated by Ni-Ti Shape Memory Alloy Wires

Filomena Simone [a,b], Daniele Meli [c], Gianluca Rizzello [a], David Naso [c],Stefan Seelecke [a,b]

[a] Department of Systems Engineering, Department of Materials Science & Engineering, Saarland University, Saarbrücken, Germany

[b] Center for Mechatronics and Automation Technologies (ZeMA) gGmbH, Saarbrücken, Germany

[c] Department of Electrical and Information Engineering, Politecnico di Bari, Bari 70125, Italy

ABSTRACT

In this paper, a dynamic model for an artificial finger driven by Shape Memory Alloy (SMA) wires is presented. Due to their high energy density, these alloys permit the realization of highly compact actuation solutions with potential applications in many areas of robotics, ranging from industrial to biomedical ones. Despite many advantages, SMAs exhibit a highly nonlinear and hysteretic behavior which complicates system design, modeling, and control. In case SMA wires are used to activate complex robotic systems, the further kinematic nonlinearities and contact problems make the modeling significantly more challenging. In this paper, we present a finite element model for a finger prototype actuated by a bundle of SMA wires. The commercially available software COMSOL is used to couple the finger structure with the SMA material, described via the Müller-Achenbach-Seelecke model. By means of several experiments, it is demonstrated how the model reproduces the finger response for different control inputs and actuator geometries.

Keywords: Shape Memory alloy, SMA, SMA activated finger, smart structure, Finite element simulation, Prosthetic hand.

1. INTRODUCTION

Ni-Ti based Shape Memory Alloys (SMAs) consist of active materials which undergo a phase transformation when exposed to heat [1]. This phase transformation is accompanied by a change in geometry, which can be effectively exploited for actuation. In addition, the change in temperature, phase, and geometry result in a variation in electrical resistance, which can be used for online reconstruction of material strain or load [2]. For actuation applications, SMAs are normally shaped as wire. Due to the high flexibility of SMA wires, it is possible to easily integrate them in compact systems, and generate complex motion patterns without using gearing mechanisms. In addition, the inherently high energy density of SMA material makes it suitable to generate a large amount of work from a system with reduced size. By using bundles of thin wires mechanically in parallel it is also possible to increase the bandwidth of SMA actuators in the range of Hz [3], or even more if the material is driven by high voltage pulses of short duration [4]. These features make SMAs an attractive solution for the realization of highly compact robotic solutions, with potential advantages in many fields of interest, e.g., industrial, biomedical [5].

The focus of this work is on SMA-actuated robotic hands for prosthetic applications. Different prototypes of prosthetic hands actuated by SMA wires have been presented in recent literature. In [6] Cho *et al.* introduced a 16 DOF hand prototype driven by 32 independent SMA wires. Each wire can be partially activated through a C-segmentation technique. Andrianesis *et al.* presented in [7] a 15 DOF prosthetic hand actuated by a SMA-spring mechanism. SMA wires having a diameter if 0.25 mm are adopted to drive the prototype fingers flexion motion. Kim *et al.* described in [8] a robotic hand whose fingers are driven by tendons based on smart soft composites and SMA material. Simone *et al.* presented in [3] a three-fingers hand actuated by bundles of SMA wires with a diameter of 0.1 mm, arranged in a protagonist-antagonist configuration. This paper demonstrates that the utilization of a protagonist-antagonist wire configuration, in combination with the use of bundles of small diameter SMA wires, helps to improve the SMA actuated system responsiveness.

Despite the developed prototypes have showcased the effectiveness of SMA technology in the prosthetic field, currently developed SMA hands are still not able to meet the requirements of amputees in real life applications [9]. This is mostly due to the limited SMA stroke, together with the material hysteresis which significantly complicates modeling, design, and control of the device. It is remarked how the development of software-assisted design tools, capable of predicting the system behavior based on accurate and computationally efficient mathematical models, represent an effective way to optimize the performance of SMA actuated hands. Such models need to account for SMA hysteresis, structure nonlinearities, kinematic constraints, thermo-mechanical coupling, thermal exchanges between the wires and structure, and thermal exchanges between among the different wires. Due to the highly complex nature of such phenomena, simulation tools capable to reproduce local effects have to be used, i.e., based on finite element (FE) method. In literature, a number of authors have presented on modeling and simulation of SMA wires interacting with structures, e.g., hydrofoils [10], airplane wings [11], and staples [12]. However, modeling of SMA-actuated robotic hands by means of FE tools has been investigated by a very limited number of authors. One example is the work by El-Sheikh *et al.* in [13], in which a 4-fingered SMA actuated hand is simulated in Matlab®. In this work, the SMA wire is modeled as a force acting on the finger phalanxes. Therefore, the complex material hysteresis is neglected. In general, the highly nonlinear behavior of both SMA material and robotic structure makes modeling and simulation of SMA-actuated prosthetic hands a challenging task.

In this paper we present FE dynamic modeling and simulation of a SMA-actuated finger. The investigated finger is similar to the ones used to actuate the hand presented in [3], shown in Fig.1. In particular, we aim at developing a mathematical framework which can be used to optimize the design of the hand, e.g., in terms of number of wires, wires location, and geometry. As a first step towards this goal, in this paper we focus on modeling and simulation of the dynamic behavior of a single SMA-actuated finger. The finger motion is controlled by a bundle of SMA wires working against a spring. The contraction of SMA wires due to heating induces a rotation of the upper phalanx. For this system, a thermo-mechanically coupled FE model is developed. The SMA material is described via the physics-based Müller-Achenbach–Seelecke (MAS) model [14]. A FE environment is preferred in this work, since it permits to implement and simulate local phenomena such as contact problems and kinematic constraints. After model description, experimental identification and validation are performed for different input commands and geometries.

This remainder of this paper is organized as follows. Description and FE implementation the finger prototype are presented in Section 2. The MAS model for SMA wires is then discussed in Section 3. Implementation of the overall system FE model is described in Section 4. Parametric identification and experimental validation are then carried out on the complete model (SMA wire coupled with the mechanical structure), and the results are presented in Section 5. Finally, Section 6 provides concluding remarks.

Fig. 1. Picture of SMA hand presented in [3].

2. FINGER PROTOTYPE MODEL

2.1 Finger Structure

As discussed in the introduction, the goal of our research consists of developing a FE tool for optimizing the design of the prosthetic hand developed in [3]. We point out that the design of such hand is rather complex, i.e., each finger is actuated by bundles of protagonist-antagonist SMA wires. As first step towards our goal, in this paper we focus on modeling of a simpler representative finger system, which is shown in Fig. 2. This finger prototype consists of two 3D printed phalanxes connected by a hinge joint. The first phalanx is fixed, while the second one is free to rotate around a joint, as shown in Fig. 2. Each phalanx has a hexahedral shape. Lengths of first and second phalanxes equal 200 and 50 mm, respectively, while the base is a square having a 19 mm side. The second phalanx is larger than the human one, since it represents metacarpus, middle phalanx, and bottom phalanx. Actuation is provided by a SMA-spring mechanism. It consists of a Flexinol® SMA wire (Dynalloy, Inc. Tusten, CA [15]) having diameter of 0.1 mm and length of 440 mm (in full austenite), connected to a linear spring. When heated via an electric current, the wire contracts and pulls the second phalanx, allowing it to rotate around the joint. The linear spring, attached perpendicularly to the second phalanx, restores the finger stretched position once the current is removed, as shown in Fig. 3.

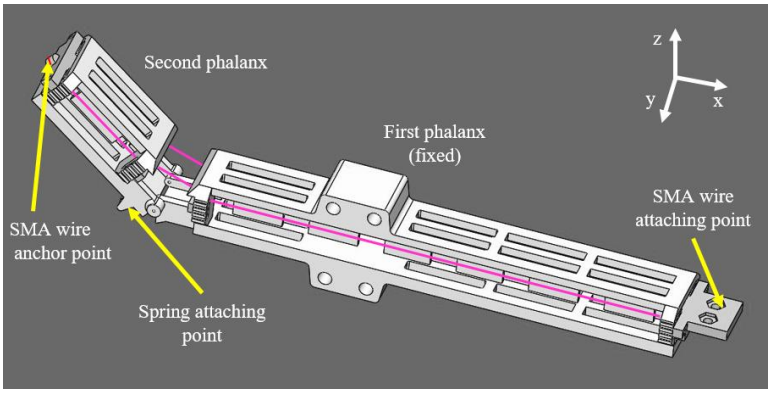

Fig. 2. Finger CAD model.

The wire is connected to the right-hand side of the first phalanx, and then wrapped along the two phalanxes around an anchor point. In this way, a bundle of two wires mechanically in parallel is obtained. In order to guide and hold the wire during the winding process, as well as during the actuation, two bores are designed at both ends of each phalanx. For maximizing the stroke, the wire is inserted in the structure in fully austenitic phase, i.e., while heated. This procedure allows to eliminate any residual strain and prestress, and also permits to mount the wire under safe stress conditions, thus improving the material lifetime [15]. Some brackets, located at the end-points of both phalanxes, allow to vary the distance between the wire and the hinge joint center of rotation. We denote this distance as r. By varying r, it is possible to modify the conversion factor between stroke/force and angle/moment. Therefore, we are interested in investigating the effect of this parameter on the actuator performance. A saw tooth pattern is designed at the ends of each phalanx, in order to ensure accurate positioning of the SMA wire with respect to the center of rotation of the second phalanx.

2.2 Finger FE Model

A model of the overall system is realized via the software COMSOL Multiphysics (COMSOL 5.2). The behavior of the finger is implemented by means of the MultiBody Dynamics (MBD) module. This module permits to simulate coupled dynamic problems involving large deformations, i.e. displacements, rotations, compliant bodies connected by joints. In addition, it permits to implement user-defined differential equations as constitutive relationships for specific elements. To achieve the FE model of the finger, the CAD Import Module is used to import in COMSOL its 3D CAD file. All the components are manufactured with hard plastic, and therefore they are modeled as rigid bodies. To constrain the second phalanx to rotate around the y-axis, a hinge joint connection is defined (see Fig. 2). The restoring spring is modeled via a spring-damper connection (not shown in Fig. 2), having a stiffness of 50 N/m and a pre-strain of 1 mm. A zero motion constraint is imposed as boundary condition for the displacement of the first phalanx, i.e., $(u_x, u_y, u_z) = (0, 0, 0)$.

3. SMA WIRE MODEL

In this work, the SMA material is described via the MAS model [14]. This model allows to simulate the behavior of a one-dimensional, single-crystal SMA system subject to a uniaxial load, within a thermodynamically consistent framework. The

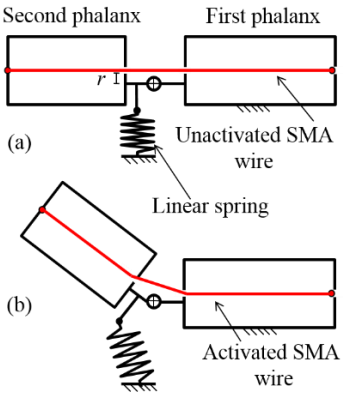

Fig. 3. SMA finger actuator, unactivated (a) and activated (b).

MAS model describes the macroscopic behavior of the material by means of considerations on mesoscopic lattice layers. In particular, it is assumed that three variants exist in the material, i.e., austenite *A* and two martensitic variants denoted as M_+ and M_-. A phase fraction is associated to each variant, i.e., x_A for *A*, x_- for M_-, and x_+ for M_+. The following consistency equation holds

$$x_A + x_+ + x_- = 1. \tag{1}$$

The kinetics of phase fractions is described by means of the following equations

$$\frac{\partial x_+}{\partial t} = -p^{+A}(\sigma,T)\,x_+ + p^{A+}(\sigma,T)\,x_A, \tag{2}$$

$$\frac{\partial x_-}{\partial t} = -p^{-A}(\sigma,T)\,x_- + p^{A-}(\sigma,T)\,x_A. \tag{3}$$

Quantity $p^{\alpha\beta}(\sigma,T)$ represent the probability for an ideal layer to overcome an energy barrier in a non-convex free-energy landscape, and transform then from phase α to phase β. Such transition probabilities can be derived via statistical thermodynamics consideration. Their analytical expression is rather complex, and thus omitted here for brevity (see [14] for details). Note that transition probabilities are functions of wire stress σ and temperature *T*. The stress σ depends on the material strain ε according to the following equation

$$\sigma = \frac{\varepsilon - \varepsilon_T\left(x_+ - x_-\right)}{\frac{\left(x_+ + x_-\right)}{E_M} + \frac{\left(1 - x_+ - x_-\right)}{E_A}}, \tag{4}$$

where E_A and E_M represent Young's moduli of austenite and martensite, while ε_T is the transformation strain. The evolution of SMA temperature is defined through the balance law of the internal energy, i.e.,

$$\rho c\frac{\partial T}{\partial t} - k\frac{\partial^2 T}{\partial x_i^2} = h\left(\frac{\partial x_+}{\partial t} + \frac{\partial x_-}{\partial t}\right) - \alpha_c S_v (T - T_E) + j, \tag{5}$$

where ρ is the material density, *c* is the specific heat, *k* is the thermal conductivity, x_i is a spatial coordinate, *h* is the latent heat of phase transformations, α_c is the heat transfer coefficient, S_v is the ratio between external surface and volume of the wire, T_E is the environmental temperature, and *j* is the volumetric density of Joule heating [16]. In particular, the first term on the right-hand side of equation (5) accounts for the rate-dependent heat generation and absorption due to the phase transformation, the second term models the heat exchange between SMA wire and external environment, and the last term represent the electric power density used as control input. Since in this work we are not interested in modeling the distribution of SMA temperature along the wire, we set $k = 0$. Therefore, quantity *T* in (5) represents the average temperature of the wire. Neglecting temperature distribution along the wire permits to significantly reduce computation

time of our FE simulations. Under this assumption, (2), (3), and (5) can be expressed as a system of ordinary differential equations (ODEs). Finally, we point out that transition probabilities also depend on transformation stresses of austenite σ_A and martensite σ_M, given as

$$\sigma_A(T) = \sigma_L + \frac{d\sigma}{dT}(T - T_L), \tag{6}$$

$$\sigma_M(T) = \sigma_A - \Delta\sigma, \tag{7}$$

where σ_L is the transformation stress from austenite to martensite at reference temperature T_L, $d\sigma/dT$ is the gradient of the transformation stress with respect to the temperature, and $\Delta\sigma = \sigma_A - \sigma_M$ represents the hysteresis width. In general, to implement the mechanical dynamics of SMA in a FE setting, the momentum balance equation is used [16]. However, such a formulation appears as unsuitable to model the mechanical coupling between SMA wire and finger structure. To overcome this problem, the constitutive equations of the SMA are implemented via a truss element. In particular, a truss can sustain only axial loads, and therefore it appears as suitable to represent the behavior of 1D SMA wires. In addition, coupling with an external system is simple in case of truss elements. The truss stress is defined in COMSOL as follows

$$\sigma_t = \sigma_{ti} + E\left(\frac{du}{dx} - \varepsilon_{inel}\right), \tag{8}$$

where σ_{ti} is the initial truss stress, E is the Young's modulus of the truss, du/dx is the truss strain, and ε_{inel} the truss inelastic strain. In order to relate the truss element to the SMA model, we have to impose that the truss stress σ_t equals the SMA stress σ in (4). This can be done by defining the following quantities

$$E = \frac{1}{\frac{(x_+ + x_-)}{E_M} + \frac{(1 - x_+ - x_-)}{E_A}}, \tag{9}$$

$$\varepsilon_{inel} = \varepsilon_T (x_+ - x_-), \tag{10}$$

$$\sigma_{ti} = 0, \tag{11}$$

$$\frac{du}{dx} = \varepsilon. \tag{12}$$

Moreover, in order to couple the SMA mechanical behavior with the phase fractions dynamics and the temperature evolution, ODEs (2), (3), (5) must be defined on the truss node.

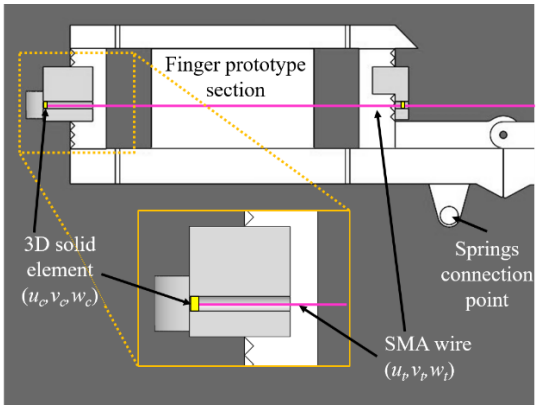

Fig. 4. Finger prototype section drawing. The SMA wire is depicted in magenta, while the 3D solid element used to build the prismatic joint is represented in yellow.

4. COMPLETE MODEL

As described in the previous section, the SMA wire is inserted in the finger structure and fixed at the end-points of the phalanxes. When a current is supplied to the wire, the SMA contracts and slides along the structure, causing a rotation of the top phalanx. In previous works, the SMA wire has been modeled with both end-points fixed to the structure, thus avoiding any relative motion [17]. Therefore, the coupling between SMA and 3D structure could be easily achieved via integration methods. In this work, on the other hand, the truss element is constrained to slide inside the bracket holes. At the same time, it has to be rigidly connected to the second phalanx. In order to achieve proper coupling between SMA and structure, some features of the MBD module are exploited. In particular, a prismatic joint relation is imposed between the truss element and the bracket holes, allowing to model the sliding motion of the wire. In order to use this feature, all the bodies involved in the coupling must be defined as solid 3D elements. For this reason, a small elastic solid element having a cylindrical shape is linked to the truss element, such that $(u_t,v_t,w_t) = (u_c,v_c,w_c)$, where (u_t,v_t,w_t) are the DOF of the truss element while (u_c,v_c,w_c) are the DOF of the solid element. The cylinder is rigidly connected to the truss, and only plays a passive role. This is shown in Fig. 4, in which the SMA wire is depicted in magenta, while the 3D solid element is depicted in yellow. The same feature is also implemented in correspondence of the other holes, for a total of 4 cylinders for each truss. To model the SMA bundle, a truss element is defined for each wire within the bundle itself. Therefore, of two trusses and eight cylindrical solid elements are defined in total. Due to its limited length, the wire part routed around the anchor point is omitted from the model. For this reason, all trusses are fixed at the tip of the second phalanx, defining zero displacement constrains in the corresponding truss nodes ($u^i_t=0$). As initial condition, the SMA wire is assumed in fully martensite plus state, i.e., $x_+ = 1$ and $x_A = x_M = 0$. Since all the experiments are performed in a temperature-controlled environment at 295 K, this value is chosen as initial condition for T.

5. RESULTS

5.1 Experiments

In this section, experiments used for model identification and validation are presented. When the wire is heated its phase, temperature, and geometry change, and electrical resistance varies accordingly. If the heating is controlled via a voltage source, the change in resistance will result into a change in current. Therefore, the resulting power supplied to the system will not be constant. To address this issue, a power control architecture is usually implemented. A power control is preferred to a voltage or current one, since the power is directly related to the wire temperature (see (5)). The power controller is designed with a National Instruments cRIO-9074 real-time data acquisition system programmed with LabVIEW 2012. It is implemented by means of a pulse width modulation architecture, as in [3]. The electrical commands are sent to SMA wires via a NI-9472 module working as a digital switch, capable of handling up to 30 volts with a 100 μs switch time. A NI-9472 voltage source is used to supply 28 V DC. A NI-9227 is used to acquire the current, and a NI-9229 module permits to measure the voltage. Prior to the experimental campaign, current and voltage are acquired while the switch is activated for 500 μs for each wire. This procedure permits to calculate the maximum power for each wire.

During the execution, the FPGA program computes the difference between desired and maximum power, and a duty cycle is generated accordingly. This duty cycle is then used to achieve PWM control of the NI-9472 switches, with a switching frequency of 100 Hz. During testing, a host desktop computer running LabVIEW generates a desired power profile for the wires, and stores the measured voltage, current, resistance, and power simultaneously. During data acquisition, the host is interfaced with a Logitech web camera, positioned perpendicularly to the finger phalanxes, which records a video at 30 frames per second.

At the beginning of each experiment, the finger is in its fully stretched position at room temperature (295 K), and the SMA is not activated. In this configuration, the angle is zero. At $t = 3$ s, the PWM controller starts to supply an increasing power profile to the wire, which generates a rotation of the phalanx. The resulting power stays then constant until $t = 13$ s. Then, the power starts to decrease in order to let the finger restore its original position. The duration of the increasing/decreasing ramps of each power signal is equal to 2 s. This experiment is repeated with different distances between the wire and the hinge joint center of rotation. By keeping the same input power, increasing this distance leads to a reduction of the resulting bending angle.

The video acquired during the experiments is post-processed with Matlab 2015, in order to reconstruct the bending motion related to the chosen input profile. To obtain the bending angle data, functions embedded in the Image Processing Toolbox and based on the gradient variation are used. In particular, the adopted algorithms permits to track the position of a point of interest properly defined within the structure, via a combination of predictions and measurements.

5.2 Parameter Identification and Validation

The parametric identification is performed on the overall system (SMA wire coupled with the finger), and aims at finding the model parameters which make measured and predicted angles as close as possible for a given calibration test. Different experiments obtained for various power inputs and different distances between wire and center of rotation (denoted as r) are conducted. Simulations are performed with PC with an Intel® Core i7 4790 processor, having clock frequency of 3.60 GHz and RAM of 32 GB.

Table 1. Values of Model Parameters

Model Variables			
Arbitrary values			
Model Variable Name	***Symbol***	***Value***	***Unit***
Trasformation strain	ε_T	0.04	-
Modulus of austenite	E_A	50	GPa
Heat convection coefficient	α	200	W/m^2
Specific heat	c	500	J/kg
Latent heat of phase transformation	h	25	kJ/kg
Optimized values			
Model Variable Name	***Symbol***	***Value***	***Unit***
Width of stress-strain hysteresis	$\Delta\sigma$	52	MPa
Austenitic transformation stress	σ_L	1	MPa
Gradient transformation stress respect to the temperature	$d\sigma/dT$	4	MPa/K
Reference temperature	T_L	320	K
Modulus of martensite	E_M	30	GPa

In the model described in Section 3, there are 10 unknown parameters which require identification, i.e., E_A, E_M, ε_T, σ_L, T_L, $\Delta\sigma$, $d\sigma/dT$, α, c and h. In principle, most of these material parameters are listed in the producer datasheet [15]. However, we point out that the SMA undergoes an additional thermo-mechanical training when embedded in a structure. This training produces some changes to the material hysteresis. Therefore, material parameters have to be properly fine-tuned in order to accurately reproduce the new operating condition. For the calibration procedure, a slow test (0.015 Hz) corresponding to a wire-joint distance r = 1.5 mm is used. In this way, the test can be assumed as quasi-stationary, so that all time derivatives can be considered as approximately zero. Under this assumption, (5) implies that the resulting temperature is proportional to the applied power. In this way, the effects of c and h can be neglected, and the identification of the remaining parameters becomes simpler. To further assist the identification process, a sensitivity analysis is performed on the model in order to understand which parameters mostly affect the finger motion.

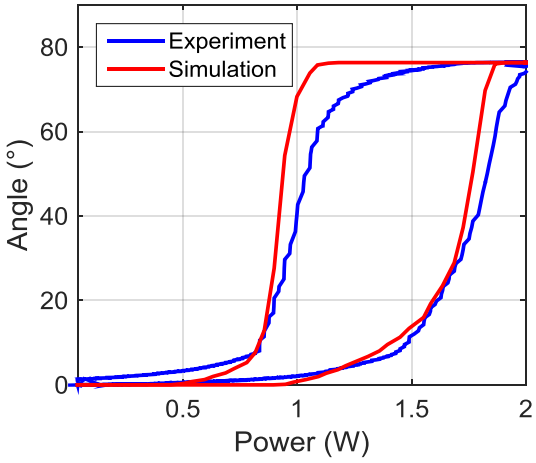

Fig. 5. Model calibration experiment, r = 1.5 mm, sinusoidal power signal at 0.015 Hz, experiment (blue line), simulation (red line).

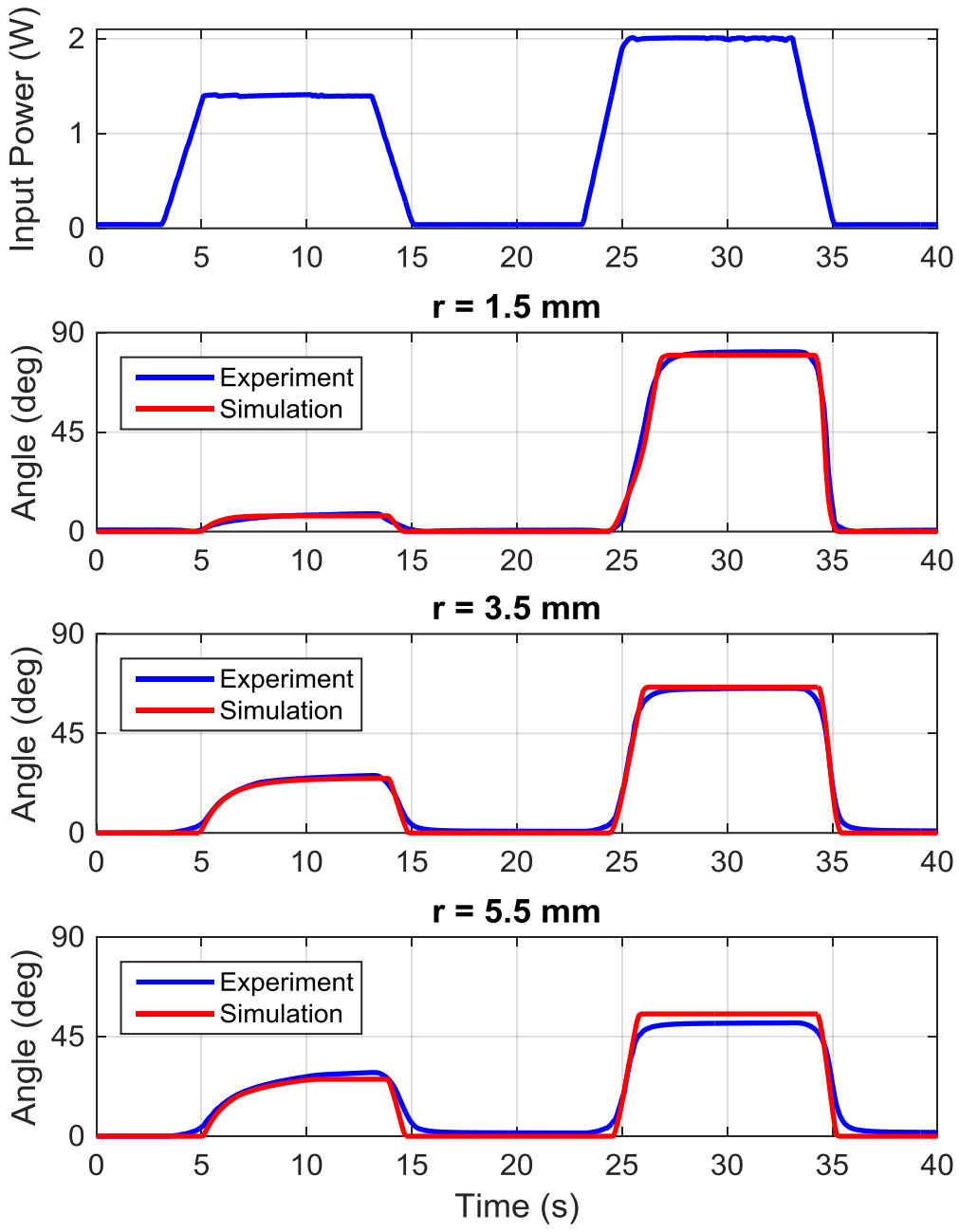

Fig. 6. Model validation experiments, r = 1.5, 3.5, 5.5 mm, trapezoidal power signal at 1.4, 2 W, experiment (blue line), simulation (red line).

Discussion on this sensitivity analysis is omitted for conciseness. As a result, parameters E_M, T_L, σ_L, $\Delta\sigma$, $d\sigma/dT$ are chosen for the optimization, while the other variables are arbitrarily fixed to conventional values, and are reported in Table I [2]. The parametric identification is implemented in COMSOL by using the Optimization module. The solution method known as Coordinate Search is chosen for addressing the optimization, i.e., a gradient-free solver capable of exploring the parameter space by avoiding local minima. To enhance the solver convergence, an admissible range is selected for each parameter according to physical considerations, as follows: $E_M \in$ [15, 35] GPa, $T_L \in$ [295, 395] K, $\Delta\sigma \in$ [40,150] MPa, $\sigma_L \in$[0.5,50] MPa, $d\sigma/dT \in$[4 7] MPa/K. The initial values used at the beginning of the optimization process are reported in Table I, and are based on experiments performed in previous works [2]. The optimized input-output hysteresis obtained

from the identification test is shown in Fig. 5. The model is capable of reproducing the global hysteretic behavior with satisfactory accuracy. The difference between experimental and simulated curves is mostly due to the adopted material model, which is based on a single-crystal approximation of the SMA behavior. In particular, it can be noted that the agreement between measured and the simulated hysteresis is satisfactory for low power values, while the error increases for intermediate powers. After parametric identification, model validation is performed by considering experiments obtained for all values of *r* and for different input powers. In Fig. 6, the comparison between experiments and simulations is shown for three different values of *r*, i.e., 1.5 mm, 3.5 mm, and 5.5 mm, and two power levels, i.e., 1.4 W and 2 W. In the same figure, the corresponding input power signal is reported. By comparing experiments and simulations, it is possible to observe a satisfactory agreement between the trends. It can be noted how the angle converges to a steady-state value with a different time constant for each power level, due to the nonlinearity introduced by the material hysteresis. As it can be observed from Fig. 6, the model well captures this effect. Note also that use of the single-crystal SMA model introduces a sharp transient behavior for the angle, which is more evident for the 2 W input power. The simulations show an increasing error in predicting the maximum bending angle value for larger values of wire-joint distance *r*. This may be due to an intrinsic limitation of the adopted model, which is based on single-crystal assumptions. Nevertheless, the overall accuracy is still satisfactory for all experiments, with a maximum error of 4 deg obtained for the 2 W, r = 5.5 mm case. Such an error is within the range of measurement errors for the adopted measurement setup, caused by noise in the digital image acquisition. The error also increases by applying intermediate power levels (results are not shown for conciseness). This is, once again, due to the approximation of material behavior caused by the single-crystal assumption.

6. CONCLUSIONS

In this work, a finite element dynamic model for a SMA-actuated finger prototype has been presented. The developed model represents the first step towards the development of a simulation framework to be used for structural system optimization. At first, the finger structure has been presented, and its COMSOL model implementation has been described. Then, a simplified version of the MAS model for the SMA wire has been discussed, together with its COMSOL implementation. A procedure to couple the 3D structure with the wire has then been presented. Different experiments have been performed by varying the prototype geometry, i.e., the distance between SMA wire and the phalanx center of rotation, as well as the input power. Experimental measurements have been compared with simulation results, providing a satisfactory agreement. The use of a simplified SMA model based on single-crystal assumptions introduces some errors in the predictions. In particular, the maximum error between simulations and experiments is of 4 deg for the 2 W, r = 5.5 mm. In addition, the error between simulations and experiments increases for power values between 1.4 W and 2 W. This issue is, once again, due to the single-crystal nature of the SMA model, which does not allow for quantitative predictions in case of materials with highly smooth (polycrystalline) hysteresis.

In future works, a computationally-efficient polycrystalline version of the SMA model will be implemented in order to improve accuracy for intermediate power levels. At the same time, phenomena such as friction, temperature gradient, and thermal exchange will be introduced in the FE model, in order to improve the prediction capabilities. Finally, the model will be used to describe the complete hand prototype described in [3], based on protagonist-antagonist SMA wires configurations.

REFERENCE

[1] Lagoudas, D. C., [Shape Memory Alloys: Modeling and Engineering Applications], Springer (2008).

[2] Furst, S. J. and Seelecke, S., "Modeling and experimental characterization of the stress, strain, and resistance of shape memory alloy actuator wires with controlled power input", *J. Intell. Mater. Syst. Struct.*, 23(11), 1233–1247 (2012).

[3] Simone, F., Rizzello, G. and Seelecke, S., "Metal muscles and nerves—a self-sensing SMA-actuated hand concept," *Smart Mater. Struct.*, 26(9), 95007 (2017).

[4] Vollach, S., Shilo, D. and Shlagman, H., "Mechanical Response of Shape Memory Alloys Under a Rapid Heating Pulse-Part II", *Experimental Mechanics*, 56 (8), 1465-1475 (2016).

[5] Furuya, Y. and Shimada, H., "Shape memory actuators for robotic applications," *Materials & Design*, 12 (1), 21-28 (1991).

[6] Cho, J. K., Rosmarin, J. and Asada, H., "SBC hand: a lightweight robotic hand with an SMA actuator array implementing C-segmentation," *IEEE International Conference on Robotics and Automation*, 921-926 (2007).

[7] Andrianesis, K. and Tzes, A., "Development and control of a multifunctional prosthetic hand with shape memory alloy actuators," *Journal of Intelligent & Robotic Systems*, 78 (2), 257-289 (2015).

[8] Kim, H. I., Han, M. W., Song, S. H. and Ahn, S.-H., "Soft morphing hand driven by SMA tendon wire," *Compos. Part B Eng.*, 105, 138–148 (2016).
[9] Biddiss, E., Beaton, D. and Chau, T., "Consumer design priorities for upper limb prosthetics," *Rehabil. Assist. Technol.*, 2 (6), 346–357 (2009).
[10] Garner, L. J., Wilson, L. N., Lagoudas, D. C. and Rediniotis, O. K., "Development of a shape memory alloy actuated biomimetic vehicle," *Smart Mater. Struct.*, 9 (5), 673 (2000).
[11] Terriault, P., Viens, F. and Brailovski, V., "Non-isothermal finite element modeling of a shape memory alloy actuator using ANSYS," *Comput. Mater. Sci.*, 36, (4), 397–410, (2006).
[12] Jaber, M. B., Smaoui, H. and Terriault, P., "Finite element analysis of a shape memory alloy three-dimensional beam based on a finite strain description," *Smart Mater. Struc.*, 17 (4), 045005 (2008).
[13] El-Sheikh, M. A., Taher, M. F. and Metwalli, S. M., "New optimum humanoid hand design for prosthetic applications," *Int. J. Artif. Organs*, 35, 251–262 (2012).
[14] Seelecke, S. and Müller, I.,"Shape memory alloy actuators in smart structures: Modeling and simulation," *Appl. Mech. Rev.*, 57 (1), 23–46 (2004).
[15] Dynalloy, "Technical Characteristics of FLEXINOL ® Actuator Wires." Available: http://dynalloy.com/pdfs/TCF1140.pdf.
[16] Furst, S., Crews, J. and Seelecke, S., "Numerical and experimental analysis of inhomogeneities in SMA wires induced by thermal boundary conditions," *Contin. Mech. Thermodyn.*,24 (4), 485–504 (2012).
[17] Yang, S. and Seelecke, S., "FE analysis of SMA-based bio-inspired bone–joint system", *Smart Mater. Struct.*, 18 (10), 104020 (2009).